

Dissecting the active galactic nucleus in Circinus IV. MUSE NFM observations unveil a tuning-fork ionised outflow morphology

D. Kakkad^{1,*}, M. Stalevski^{2,3}, M. Kishimoto⁴, S. Knežević², D. Asmus^{5,6}, F. P. A. Vogt⁷

¹Space Telescope Science Institute, 3700 San Martin Drive, Baltimore, MD 21218, USA

²Astronomical Observatory, Volgina 7, 11060 Belgrade, Serbia

³Sterrenkundig Observatorium, Universiteit Gent, Krijgslaan 281-S9, Gent, 9000, Belgium

⁴Department of Astrophysics & Atmospheric Sciences, Faculty of Science, Kyoto Sangyo University, Kamigamo-motoyama, Kita-ku, Kyoto 603-8555, Japan

⁵Department of Physics & Astronomy, University of Southampton, Southampton, SO17 1BJ, UK

⁶Gymnasium Schwarzenbek, 21493 Schwarzenbek, Germany

⁷Federal Office of Meteorology and Climatology - MeteoSwiss, Chemin de l'Aérologie 1, 1530 Payerne, Switzerland

Accepted XXX. Received YYY; in original form ZZZ

ABSTRACT

We present the ionised gas outflow morphology in the Circinus galaxy using the Narrow Field Mode (NFM) of the MUSE instrument on board the Very Large Telescope (VLT). The NFM observations provide a spatial resolution of $\sim 0.1''$, corresponding to a physical scale of ~ 2 pc, one of the highest spatial resolution achievable using ground-based AO-assisted observations in the optical wavelengths. The MUSE observations reveal a collimated clumpy outflow profile originating near the AGN location and extending up to $1.5''$ (~ 30 pc) in the NW direction. The collimated structure then fragments into two filaments, giving the entire outflowing gas a “tuning-fork” morphology. These structures remain undetected in the lower spatial resolution MUSE Wide Field Mode data. We explain the origin of this tuning-fork structure to the interaction of the outflow with a dense clump in the interstellar medium (ISM) as the outflow propagates outward. The origin of the collimated structure itself could be from jet-ISM interactions on small scales. These observations also provide evidence to the origin of the ionised gas filaments previously observed in the Circinus galaxy out to kiloparsec scales. We find instantaneous and time-averaged mass outflow rates of $10^{-2} M_{\odot} \text{ yr}^{-1}$ and $10^{-4} M_{\odot} \text{ yr}^{-1}$, respectively. Based on the star formation rate in the Circinus galaxy reported in the literature, the observed ionised outflows are not expected to regulate star formation within the ~ 100 pc scales probed by the NFM data.

Key words: galaxies:active – galaxies:individual – galaxies:ISM – galaxies: kinematics and dynamics – galaxies: nuclei – galaxies: Seyfert

1 INTRODUCTION

The so-called Unified Model (UM) of the active galactic nuclei (AGN) consists of a central black hole surrounded by an equatorial torus-like structure, which is responsible for the angle-dependent obscuration of the accretion disk and in some cases, may include collimated jets along the polar directions (e.g., Antonucci 1993; Urry & Padovani 1995; Netzer 2015). The equatorial torus has been believed to dominate the infrared emission from the AGN (see Ramos Almeida & Ricci 2017, and the references therein). There have been intensive efforts in the literature, both from an observational as well as modelling perspective, to study the nature of this torus, such as its geometry (e.g., Hönic 2019; García-Burillo et al. 2021), what are the typical dust covering factors (e.g., Elitzur 2012; Stalevski et al. 2016; Toba et al. 2021) and whether the material is clumpy or smooth (e.g., Dullemond & van Bemmell 2005; Marin et al. 2015; García-González et al. 2017).

High resolution mid-infrared observations over the past decade have now challenged these simplified torus model that have dusty

clumps only in the equatorial region (Nenkova et al. 2002). Several studies in the literature now show strong infrared emission along the polar direction on the scales of a few parsecs (e.g., Hönic et al. 2012, 2013; López-Gonzaga et al. 2016; Hönic & Kishimoto 2017; Leftley et al. 2018) to hundreds of parsecs (e.g., Braatz et al. 1993; Bock et al. 2000; Asmus et al. 2016; Asmus 2019). As a result, the dust emission around the AGN is believed to consist of two components: an equatorial thin disk and a polar extended feature that could originate from the winds from the central engine (see Hönic 2019, and the references therein).

The polar wind is believed to have a multi-phase composition ranging from dust to ionised and molecular gas components. In fact, recent high spatial resolution observations of nearby AGN have targeted the molecular gas distribution around the torus using ALMA, revealing high velocity outflows in the molecular gas phase (e.g., Gallimore et al. 2016; Combes et al. 2019; García-Burillo et al. 2019; Lopez-Rodriguez et al. 2020). In order to get a holistic view of the multi-phase dusty gas flows around the torus, it is imperative to obtain the morphology and kinematics of the ionised gas on the same scales as the molecular gas and infrared emission. Furthermore, obtaining outflow morphology at such small spatial scales can also

* E-mail: dkakkad@stsci.edu

give clues into the outflow launching mechanism and connect them to the observed kiloparsec scales structure or outflows, whenever available in the literature. Thanks to the Narrow Field Mode (NFM) capabilities of the Multi Unit Spectroscopic Explorer (MUSE [Bacon et al. 2010](#)) at the Very Large Telescope (VLT), such high spatial resolution observations can now be performed with ground-based Integral Field Spectroscopic instruments operating at optical wavelengths. The optical wavelengths provide access to bright emission lines such as the $[\text{O III}]\lambda 5007$ that trace ionised gas in the Narrow Line Region (NLR). Furthermore, emission lines such as $\text{H}\alpha$, $\text{H}\beta$, $[\text{N II}]\lambda\lambda 6549, 6585$ and $[\text{S II}]\lambda\lambda 6716, 6731$ help derive dust extinction maps and diagnostic diagrams that trace the source of ionisation across the field-of-view.

The Circinus galaxy is the closest Seyfert 2 galaxy (~ 4.2 Mpc away, $z = 0.001$ [Freeman et al. 1977](#)) and hosts an infrared-bright AGN (e.g., [Jarrett et al. 2019](#)). The polar axis of the AGN in the Circinus galaxy is seen almost edge-on and is therefore an ideal target to study the relative gas and dust structure in a typical obscured AGN. Recent mid-infrared (MIR) observations using the upgraded VISIR instrument at the Very Large Telescope (VLT) suggests the presence of dust in the form of a hollow cone at the edges of the ionised outflow (e.g., [Stalevski et al. 2017](#)). The polar elongation of the infrared emission has also been reported on parsec scales (e.g., [Tristram et al. 2014](#); [Stalevski et al. 2019](#)) using Mid-Infrared Interferometric Instrument (MIDI) and the Multi AperTure mid-infrared Spectroscopic Experiment (MATISSE, e.g., [Isbell et al. 2022](#)) at the VLT. The presence of dust in the form of a hollow cone in the polar region is also confirmed by multi-band optical polarimetry with VLT/FORS2 ([Stalevski et al.](#), submitted). The galaxy also hosts powerful outflows in the ionised gas phase, visible in the form of a one-sided ionisation cone extended up to ~ 1 kiloparsec (e.g., [Marconi et al. 1994](#); [Veilleux & Bland-Hawthorn 1997](#); [Mingozzi et al. 2019](#); [Fonseca-Faria et al. 2021](#); [Kakkad et al. 2022](#)). The Circinus galaxy hosts an obscured AGN with nuclear star formation that dominates the dust emission on scales of hundreds of parsec (e.g., [Matt et al. 2000](#); [Arévalo et al. 2014](#)).

In this fourth paper in the series, we map the morphology and kinematics of ionised gas in the Circinus galaxy at ~ 2 pc resolution using MUSE-NFM observations. We present a model of the ionisation cone and the resulting outflowing gas structure. The observed ionised outflow morphology obtained from the NFM observations is compared with the larger scale outflows observed with the Wide Field Mode (WFM) of MUSE, to understand outflow propagation across the host galaxy. We locate the regions with high dust extinction and compare this with the archival mid-infrared images. Lastly, the MUSE data is compared with other archival radio observations to infer the presence of jet-ISM interaction in the host galaxy.

Throughout this paper, we adopt the following Λ CDM cosmological parameters: $H_0 = 70 \text{ km s}^{-1}$, $\Omega_M = 0.3$ and $\Omega_\Lambda = 0.7$. All the maps use the following convention: North is up and East is to left.

2 MUSE-NFM OBSERVATIONS & DATA REDUCTION

The observations were performed using the Laser Tomographic Adaptive Optics (LTAO) assisted Narrow Field Mode of the MUSE instrument, on board Unit Telescope 4 of the VLT¹. The observations were carried out on the nights of 29 and 30 April 2019 with a DIMM seeing in the range $0.89\text{--}1.01''$. We observed the galaxy with

an optimised sequence: O-S-O-O-S-O (O = Object, S = Sky), where the Sky was obtained at an offset position ~ 1.5 arcmin away outside the galaxy. We performed small dithering between the individual science exposures and rotated the field by 90 degrees on each subsequent exposure to eliminate the impact of bad pixels and to average out the patterns of slicers and channels. The nucleus of the Circinus galaxy has an H-band magnitude of 13.4 and therefore, served as the Adaptive Optics (AO) reference for the Wavefront Sensor (WFS). The total on-source exposure time was ~ 4000 s.

The raw data was reduced using the standard MUSE pipeline (e.g., [Weilbacher et al. 2014, 2020](#)). The pipeline performs bias correction, flat fielding, wavelength and astrometry calibration, sky subtraction and flux calibration. The final data cube consisted of a field-of-view of $\sim 7.5 \times 7.5 \text{ arcsec}^2$ centred on the nucleus (AGN) with a spatial sampling of $0.025''$. As the observations were performed in the Nominal mode, this provided a uniform wavelength coverage between $4800\text{--}9300 \text{ \AA}$ with a gap between $5780\text{--}6050 \text{ \AA}$ due to the presence of a notch filter that suppresses the Sodium laser light. The spectral PSF (also known as the Line Spread Function, LSF) is in the range $2.5\text{--}2.9 \text{ \AA}$, with the best resolution obtained at the redder end of the spectra. This corresponds to a velocity resolution of $\sim 150 \text{ km s}^{-1}$ at the location of $[\text{O III}]\lambda 5007$ line, one of the emission lines that will be analysed in this paper. The LTAO-assisted observations resulted in a spatial PSF of $\sim 0.1''$, determined using one of the point sources in the field-of-view. This spatial resolution is one of the highest that can be achieved using ground-based IFS observations. At the redshift of the Circinus, this corresponds to a physical scale of ~ 2 pc, which means that the observations can potentially resolve the region near the AGN torus. With a field-of-view of $7.5'' \times 7.5''$, the NFM observations trace spatial scales up to ~ 100 pc from the AGN location.

3 ANALYSIS

In order to derive the flux and velocity maps from the optical emission lines, we first subtract the stellar continuum emission across the MUSE field-of-view. We perform the stellar continuum emission using the LZIFU tool (e.g., [Ho et al. 2016](#); [Kreckel et al. 2018](#)), which adopts the penalized pixel fitting routine (PPXF [Cappellari & Emsellem 2004](#); [Cappellari 2017](#)) to fit the stellar continuum using input stellar spectrum templates (from [González Delgado et al. \(2005\)](#)) or modelled simple stellar populations (SSPs) that are convolved with parametrised velocity distributions. In doing so, regions in the spectra with strong skylines and emission lines intrinsic to the host galaxy were masked. The key emission lines that were masked were $\text{H}\beta$, $[\text{O III}]\lambda\lambda 4959, 5007$, $[\text{N II}]\lambda\lambda 6549, 6585$, $\text{H}\alpha$ and $[\text{S II}]\lambda\lambda 6716, 6731$ ($[\text{S II}]$ doublet hereafter). We also mask the notch filter region in the spectrum that is contaminated by the sodium doublet emission from the lasers. Being a Seyfert 2 galaxy, the Circinus galaxy does not display broad emission lines from the Broad Line Region (BLR).

The resulting stellar continuum-subtracted data cubes were then used to analyse the morphology, kinematics and the ionisation mechanism of the gas using strong emission lines in the optical spectra. For instance, we used the $[\text{O III}]\lambda 5007$ line ($[\text{O III}]$ hereafter) to trace the ionised gas in the Narrow Line Region (NLR), the Balmer lines $\text{H}\alpha$ and $\text{H}\beta$ lines are used to trace potential star formation and dust extinction in the host galaxy (using Balmer decrement), the $[\text{N II}]\lambda\lambda 6549, 6585$ lines are used in investigating the ionisation source in each pixel (AGN or star formation) and the $[\text{S II}]$ doublet are used to trace the ionised gas electron density. We model these emission lines with multiple Gaussian functions using the `scipy.curve-fit` package in

¹ ESO programme ID: 0103.B-0396(A)

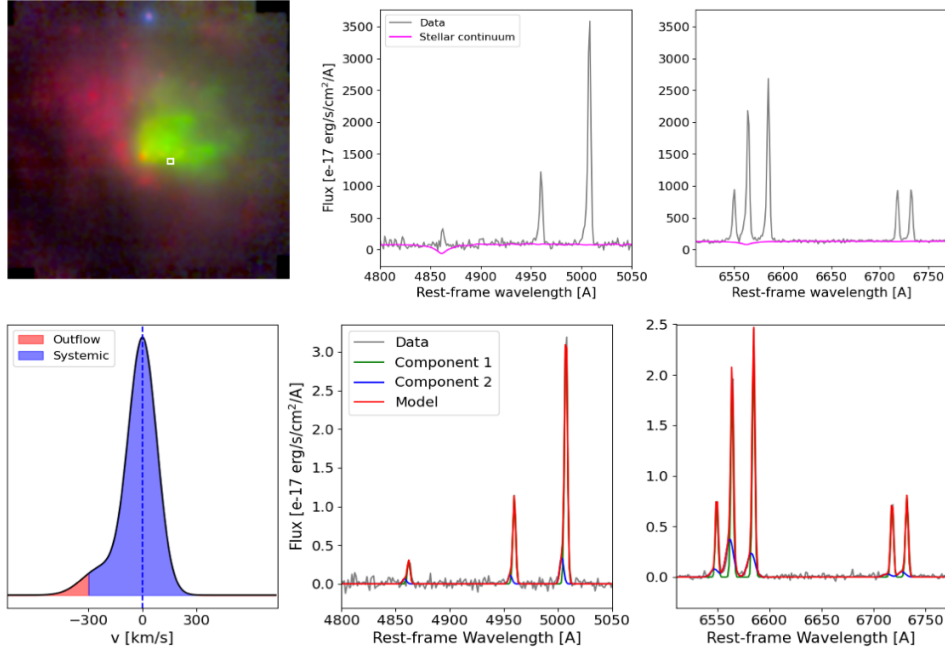


Figure 1. The top left panel shows an RGB colour image of the Circinus galaxy, derived from the NFM data. The field-of-view of the RGB image is $7.5'' \times 7.5''$. The red hue indicated the $H\alpha$ emission, while the ionised gas cone is apparent in green. The white square at the edge of the ionisation cone shows the pixel from where the example spectra shown in this figure was obtained. The middle and right panels in the top row shows the example of a stellar continuum fit and the middle and right panels in the bottom row shows the emission line fitting results of $H\beta$, $[O\text{ III}]\lambda\lambda 4959, 5007$, $[N\text{ II}]\lambda\lambda 6549, 6585$, $H\alpha$ and $[S\text{ II}]\lambda\lambda 6716, 6731$. In all the spectra, the grey curve shows the extracted data from the pixel location shown in the median image, the magenta curve shows the stellar continuum model, the green and blue curves show the individual Gaussian components used to model the emission lines and the red curve shows the overall model. The bottom left panel illustrates the definition of outflow and systemic flux used in this paper. Further details are given in Sect. 3.

python (see Virtanen et al. 2020). Initially a single Gaussian is fitted to the emission line profile, and additional Gaussian functions were added if the χ^2 is minimised, and until the line fluxes are stable within $\sim 10\%$. Circinus does not display BLR emission in its $H\beta$ or $H\alpha$ profiles and the maximum number of Gaussians required to model an emission line was two. We do not assign any physical significance to the individual Gaussian components as we follow a non-parametric approach to derive the properties associated with the systemic and outflow components. The non-parametric approach was chosen over a parametric model as it does not depend on the choice of the models used for the emission lines (e.g., Gaussian, Lorentzian or a power-law). In addition, we tied the line centroids of $[O\text{ III}]\lambda 5007$ line with that of $H\beta$ and the $[N\text{ II}]\lambda 6585$ and $[S\text{ II}]\lambda 6731$ lines with that of $H\alpha$ based on the expected location of the respective atomic species. The emission line ratios $[O\text{ III}]\lambda 5007:[O\text{ III}]\lambda 4959$ and $[N\text{ II}]\lambda 6585:[N\text{ II}]\lambda 6549$ were set approximately equal to 3:1 based on expectations from theory (e.g., Osterbrock & Ferland 2006; Dimitrijević et al. 2007). Lastly, the FWHM of the individual Gaussian components of the $[O\text{ III}]\lambda 5007$ line was coupled with $H\beta$ and the $H\alpha$ FWHM with that of $[N\text{ II}]\lambda 6585$.

From the line fitting procedure, we are interested in the following parameters: The 10th percentile velocity: v_{10} (blue-shifted $[O\text{ III}]\lambda 5007$ velocity that contains 10% of the overall $[O\text{ III}]\lambda 5007$ flux), the width of the emission line: w_{80} (width containing 80% of the flux of the emission line, see Harrison et al. 2014; Kakkad et al. 2016; Wylezalek et al. 2020) and the flux of the outflowing and systemic components of each of the emission lines. To determine the fluxes, we first define the zero velocity location in the emission line spectra, which is the location of the peak of the emission line. The flux within $\pm 300\text{ km s}^{-1}$ on either side of this zero velocity location is considered to be the systemic component of the emission line. The choice of 300 km s^{-1}

is based on the line width (FWHM) cut of $\sim 600\text{ km s}^{-1}$ which is often employed in the literature to distinguish between outflowing and non-outflowing gas (e.g., Kakkad et al. 2020). Using similar arguments, we use the flux outside of the $\pm 300\text{ km s}^{-1}$ channels to define the flux associated with outflows. Using lower velocity cuts such as 250 or 200 km s^{-1} yield similar results, but due to the possibility of contamination from the non-outflowing gas at the lower velocities, we make a conservative cut of 300 km s^{-1} . Figure 1 shows an example of the analysis methods and the fitting results presented in this section.

4 RESULTS & DISCUSSION

In this section, we show the results of the analysis methods described in Sect. 3. The main aim of this section is to derive the ionised gas outflow morphology and kinematics close to the AGN torus and compare this with archival multi-wavelength data, including the low spatial resolution MUSE-WFM data.

4.1 The parsec-scale ionised outflow in the Circinus galaxy

Figure 2 shows the flux maps of the systemic (left panel) and outflowing component (middle panel) of the $[O\text{ III}]\lambda 5007$ emission line from the NFM data. The systemic $[O\text{ III}]\lambda 5007$ flux map traces the ionisation cone originating from the AGN location and extends towards the NW direction from the nucleus. The presence of the ionisation cone in the Circinus galaxy has previously also been reported in the literature, including MUSE Wide Field Mode (WFM) observations (e.g., Marconi et al. 1994; Fischer et al. 2013; Mingozi et al. 2019; Fonseca-Faria

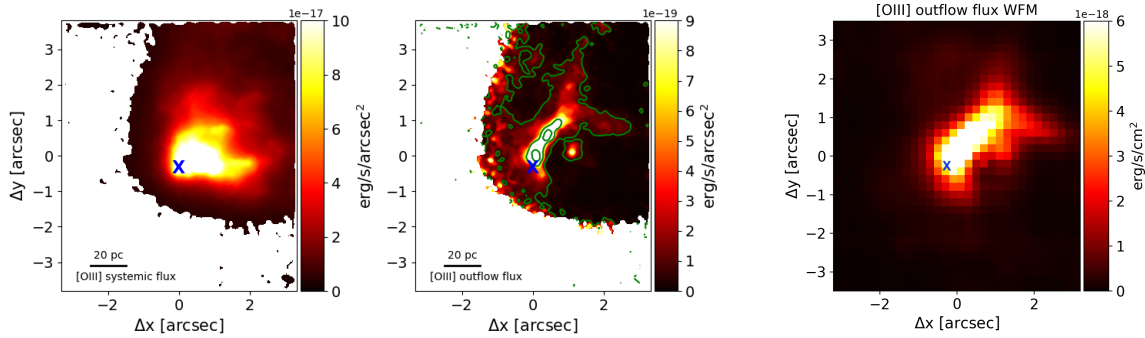


Figure 2. The left panel shows the systemic [O III] flux ($|v| < 300 \text{ km s}^{-1}$) that traces the ionisation cone. The middle panel shows the outflowing component of the [O III] flux ($|v| > 300 \text{ km s}^{-1}$). The outflow morphology suggests the gas propagation along a collimated structure before it fragments into two filaments, giving it a "tuning-fork" resemblance. The green contours in the middle panel shows the [O III] outflow contours within the collimated structure to highlight that the outflowing structure itself shows the presence of clumps. Thanks to the $0.1''$ spatial resolution achieved with the NFM observations, such structures are barely visible in archival WFM data shown in the right panel. In all the panels, the blue "X" marks the AGN location and the black bar on the bottom left shows the 20 pc scale.

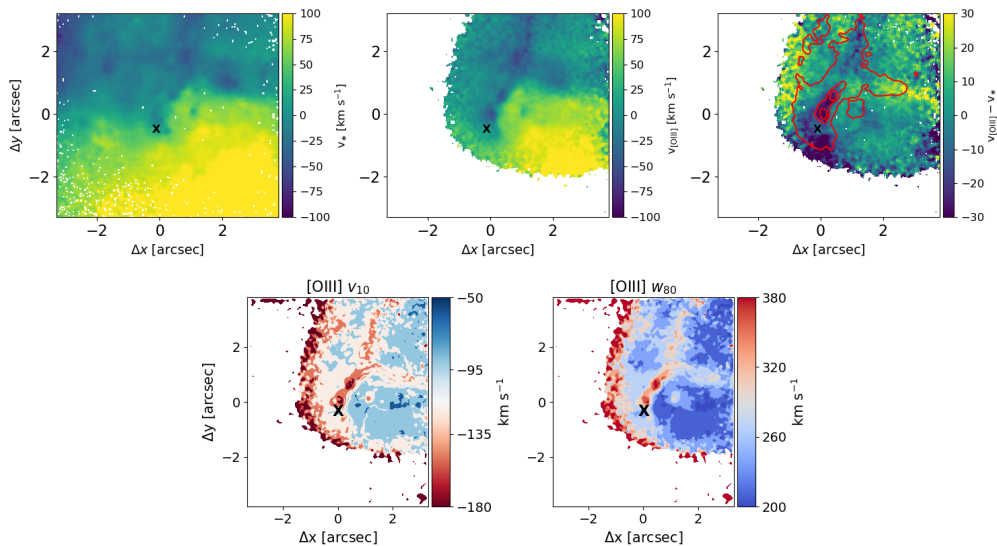


Figure 3. The top left panel shows the stellar velocity map obtained from the stellar continuum fitting. The stellar velocity map shows a smooth rotation-like profile of the host galaxy. The [O III] centroid velocity profile (top centre panel) approximately mimics the stellar velocity field, suggesting that the bulk of the ionised gas cone co-rotates with the host galaxy. The top right panel shows the residual map after subtracting the stellar velocity map from the [O III] velocity map. We observe residuals at the locations of the "tuning-fork" structure (red contour), suggesting that it is a part of the non-rotation component. The positive residuals in the filament directed towards the West and the negative residuals in the filament towards North shows that the outflow itself is co-rotating with the ionised gas and the host galaxy. The bottom panels show the non-parametric velocities, v_{10} and w_{80} , described in Sect. 3. Both these velocities confirm that the high velocity regions are along the collimated structure that fragments into two filaments $\sim 1.5''$ from the AGN location. Furthermore, the presence of this structure in the v_{10} map shows that the dominant component of the outflow is blue-shifted. The black "X" in all maps indicate the AGN location.

et al. 2021; Kakkad et al. 2022). The systemic flux dominates the bulk of the ionised gas flux in the host galaxy by nearly two orders of magnitude, compared to the [O III] outflow flux. The [O III] outflow map (middle panel, Fig. 2), on the other hand, shows a collimated structure that originates close to the AGN location and extends towards the NW of the nucleus (same direction and approximately the same PA as the ionisation cone). The collimated structure itself is not uniform and shows multiple clumps. Such clumps have also been previously reported in extended radial ionised gas filaments of the Circinus galaxy (e.g., Veilleux & Bland-Hawthorn 1997). We note that the location of the first clump is not coincident with the AGN location, but $\approx 0.4''$ NW of the nucleus. In Section 5, we further dis-

cuss the origin of these clumps and whether they could be produced by the shocks within the outflowing wind.

Beyond $\sim 1.5''$ from the AGN location ($\sim 30 \text{ pc}$) in the NW direction, the collimated structure then fragments into two filaments, one towards the West and another towards North, which gives the overall outflow morphology a "tuning-fork" resemblance. The impact of the high resolution NFM observations is clear from these observations as such pc-scale filaments and fragmenting structures are not visible in the archival low resolution ($\sim 0.5''$) MUSE WFM data, as shown in the right panel of Fig. 2.

Figure 3 shows velocity maps of the stellar component and the ionised gas of the Circinus galaxy, derived from the NFM observations. The top left panel in Fig. 3 shows the stellar velocity distribution

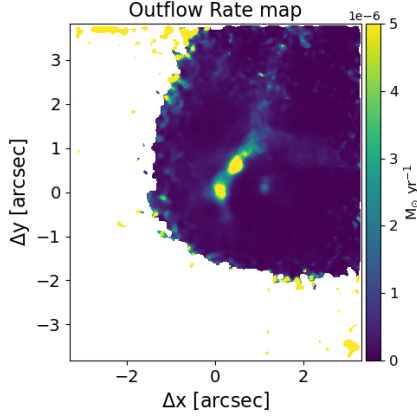


Figure 4. The map shows the mass outflow rate distribution for the ionised gas derived from the [O III]λ5007 line in the MUSE-NFM observations of the Circinus galaxy. The mass outflow rates are higher in regions with higher outflow velocity.

in the host galaxy obtained from the stellar continuum modelling. The velocity map shows a smooth gradient indicating a rotation-like profile, with the axis of rotation aligned approximately along the axis of the ionisation cone. The [O III] centroid map, shown in the top centre panel of Fig. 3, mimics the stellar velocity map i.e., the ionised gas co-rotates with the host galaxy. The [O III] centroid velocity profile is also consistent with previous MUSE-WFM results from the literature (e.g., Fonseca-Faria et al. 2021). On subtracting the stellar velocity component from the [O III] centroid velocity, we see clear residuals at the locations of the "tuning-fork" structure, as shown in the top right panel of Fig. 3. This proves that the outflow flux shown in the middle panel in Fig. 2 is indeed part of the non-systemic component of the host galaxy. Furthermore, the positive and negative residuals in the West and North arms respectively in the residual map in the top right panel of Fig. 3 indicates that the fork structure itself is co-rotating with the host galaxy and the ionisation cone. The bottom panels in Fig. 3 show the [O III] v_{10} and the w_{80} maps (left and right panels respectively). Both the v_{10} and w_{80} maps confirm the results seen in the outflow maps i.e., the high velocity regions are collimated up to $\sim 1.5''$ from the AGN location before they fragment into two filaments. The presence of the tuning-fork structure in the v_{10} map suggests that most of the observed outflow flux is dominated by the blue-shifted emission. We note that the stellar velocity map in the top left panel of Fig. 3 also shows a "V-shaped" structure at approximately the same location where the high velocity regions fragment into the two arms, suggesting that the material within the cone is both outflowing and co-rotating with the host galaxy.

We also derived the ionised gas mass outflow rate using the [O III] line adopting methods from the literature (e.g., Rupke et al. 2005; Genzel et al. 2011; Veilleux et al. 2020; Kakkad et al. 2022). We report two kinds of outflow rate values: Instantaneous outflow rates (\dot{M}_{inst}) is the sum of mass outflow rates calculated for each pixel, and time-averaged mass outflow rate (\dot{M}_{Tavg}) calculated by taking averaged quantities over the whole outflowing region. These quantities can be computed using the following equations:

$$\dot{M}_{\text{inst}} = \sum_{\text{pix}} \frac{M_{\text{out}} \cdot v_{\text{out}}}{\Delta R} \quad (1)$$

$$\dot{M}_{\text{Tavg}} = \frac{M_{\text{out}} \cdot \langle v_{\text{out}} \rangle}{R} \quad (2)$$

In Equation 1, the mass of the outflowing ionised gas, M_{out} and the velocity of the ionised gas, v_{out} is computed for each pixel and ΔR is the size of the pixel. In Equation 2, on the other hand, M_{out} is the total outflowing gas mass computed from the outflowing [O III] flux and v_{out} is the average velocity over the outflowing region ($\sim 300 \text{ km s}^{-1}$). The parameter, R , in Eq. 2 is the distance of the outflow from the AGN location. As we are using spatially-resolved observations, we do not need to assume an outflow geometry or outflow density for the time-averaged quantity. The outflow density in both cases is obtained from the flux ratio of the outflowing components of [S II]λλ6716, 6731.

The mass outflow rate map, representing the instantaneous mass outflow rates (Eq. 1), is shown in Fig. 4, where the mass outflow rate was calculated for each pixel. The advantage of using this method is that variation in the outflow parameters such as outflow density and velocity can be incorporated without the need for any assumptions on outflow models. We find the median outflow density across the field-of-view, calculated using the flux ratio of [S II]λλ6716, 6731 to be $\sim 200 \text{ cm}^{-3}$ (e.g., Sanders et al. 2016; Kaasinen et al. 2017; Kakkad et al. 2018). The total summed instantaneous outflow rate is $0.01 \text{ M}_{\odot} \text{ yr}^{-1}$ (an average of $3 \times 10^{-7} \text{ M}_{\odot} \text{ yr}^{-1}$ per pixel where outflow is detected), which is two orders of magnitude less than the total instantaneous outflow rate value reported with MUSE-WFM observations (Kakkad et al. 2022). The time-averaged outflow rate computed using Eq. 2 is $10^{-4} \text{ M}_{\odot} \text{ yr}^{-1}$. The obscured star formation rate (SFR) in the Circinus galaxy is reported to be between $3\text{--}8 \text{ M}_{\odot} \text{ yr}^{-1}$. The orders of magnitude difference between the SFR and the ionised outflow rate within a radius of $\sim 100 \text{ pc}$ of the AGN location, therefore, suggests that the observed ionised outflow is not expected to shut down star formation in the host galaxy. However, this may not be true for kiloparsec-scale molecular outflows where the outflow rate in the molecular gas phase has been reported to be $\sim 0.35\text{--}12.3 \text{ M}_{\odot} \text{ yr}^{-1}$ (see Zschaechner et al. 2016). The high molecular outflow rate in kiloparsec-scales can, therefore, regulate star formation. A multi-phase approach to high resolution gas kinematics, by tracing warm and cold molecular gas components, is required to robustly confirm whether these AGN outflows affect star formation within $\sim 100 \text{ pc}$ of the AGN.

Lastly, using spatially resolved Baldwin, Phillips & Terlevich diagrams (e.g., Baldwin et al. 1981; Veilleux & Osterbrock 1987), we infer that the dominant source of ionisation across the NFM field-of-view is the AGN and the ionisation by star formation is negligible or absent (Figure 5). The ionisation structure is consistent with previous WFM results in the literature (e.g., Mingozzi et al. 2019; Kakkad et al. 2022). The ionisation by the AGN is observed for both systemic as well as outflowing components. Therefore, the current observations also do not support a scenario where these outflows trigger star formation activity in the vicinity of the AGN.

4.2 The dust-outflow connection in Circinus

Previous mid-infrared observations of the Circinus galaxy established that a major fraction of dust emission is coming from the polar region, tentatively associated with dusty winds driven by radiation pressure (e.g., Stalevski et al. 2017; Venanzi et al. 2020). Even though far away from the central engine, dust and gas are expected to be coupled and co-spatial, and until recently the models of infrared emission ignored this polar dust component. The spatially-resolved optical spectra from the MUSE-NFM mode can be used to derive extinction maps from Balmer decrement ($H\alpha/H\beta$) to confirm the presence of dust along the polar direction. Therefore, we derived the host galaxy extinction, A_V , across the NFM field-of-view using the

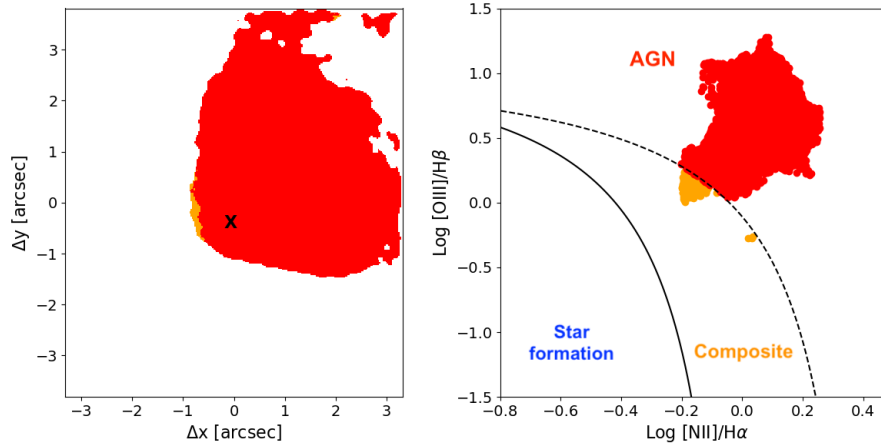


Figure 5. The left panel shows the ionisation structure (AGN in red and composite in orange) in the field-of-view probed by the MUSE-NFM data. The right panel shows the location of each pixel in the classical [N II] BPT diagram. The solid and dashed black curves are obtained from [Kauffmann et al. \(2003\)](#) and [Kewley et al. \(2001\)](#) and divide the plots between regions ionised by AGN, star formation and composite processes. The systemic flux of the emission lines was used while plotting this diagram. However, the results are similar if the outflowing components is used. The figure highlights that the gas is ionised primarily by the AGN.

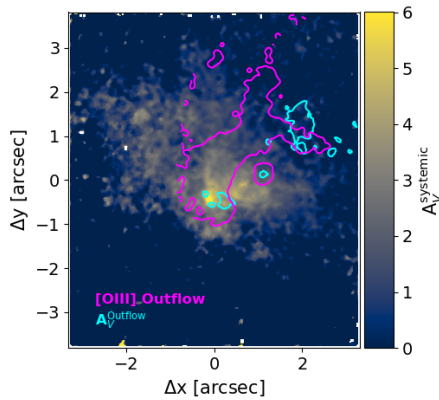


Figure 6. Dust extinction (A_V) map of the Circinus galaxy using the NFM observations. The background image shows the extinction map obtained from the systemic components of $H\alpha$ and $H\beta$, the cyan contours show the extinction from the outflowing components and the magenta contours show the location of high velocity ionised gas outflow. The dust extinction is dominant along the polar direction, consistent with previous mid-infrared observations in the literature.

Balmer Decrement parameter. We assumed a [Calzetti et al. \(2000\)](#) dust attenuation law with $R_V = 4.05$ and a fixed temperature of 10,000 K, which is the typical electron temperature in the NLR. We note that the Circinus galaxy suffers from Galactic extinction of $A_V \sim 2$ (see [For et al. 2012](#)). However, the [O III] outflow morphology and the associated velocities and mass outflow rates will not change on correcting the Galactic extinction. The extinction map is shown in Fig. 6. The background map in Fig. 6 shows the extinction map obtained from the systemic components of the flux ratio, $H\alpha/H\beta$. The cyan contours show the extinction ($A_V > 1$) obtained from the outflowing component of $H\alpha$ and $H\beta$, and the magenta contours show the location of the [O III] ionised gas outflow from the middle panel in Figure 2.

While the map in Fig. 6 shows potential dust distribution both along the disk (consistent with the results reported in [Mingozzi et al. \(2019\)](#) and [Fonseca-Faria et al. \(2021\)](#)) as well as the polar direction, the overall distribution is dominant along the polar direction. This result

is consistent with the previous results with mid-infrared emission, which was also dominant along the polar direction (e.g., [Jaffe et al. 2004](#); [Tristram et al. 2007, 2014](#); [Asmus et al. 2016](#)). This suggests that the dust along the polar direction might be a part of lower velocity gas (compared to the high velocity collimated outflow observed here) surrounding the ionised gas outflow. The extinction from the systemic components peaks at the location of the AGN and gradually falls off to $A_V = 0$ at a distance of $\approx 3''$ i.e., ≈ 60 pc.

The extinction obtained from the outflowing $H\alpha$ and $H\beta$ components shows non-uniform clumps scarcely distributed along the polar direction. We attribute these clumps to be a part of the outflowing gas and dust. It is worth noting that one of these clumps is almost at the tip of the collimated component of the outflow, approximately where the outflow filament fragments into two arms. The observation, therefore, might support a picture where the ionised gas outflow chooses the path of least resistance and therefore fragments into the two filaments, avoiding the region radially outward towards where the dust clump is present.

5 DISCUSSION

The results presented in Section 4 highlights the complex structures within an outflow that are revealed from high resolution observations in the vicinity of the AGN. The presence of an outflow in the form of an ionisation cone in the Circinus galaxy has been known for nearly three decades, and thanks to the current state-of-the-art instrumentation that we are now able to resolve parsec scale emission using optical spectra. The origin of the initial clumpy collimated structure observed in the NFM data could be due to a small-scale radio jet. The Circinus galaxy is known to host a radio jet, although its PA is aligned closer to the edge of the ionisation cone (e.g., [Elmouttie et al. 1998](#)). However, these are lower spatial resolution radio imaging observations and the regions close to the AGN torus is not resolved. Due to the precession and interaction with the surrounding medium, jets in AGN are known to bend and change directions at larger scales (e.g., as in the case of NGC 1068 [Gallimore et al. 2004](#)). Therefore, future work will target the regions closer to the AGN to search for the potential impact of small-scale jets that may be aligned along the

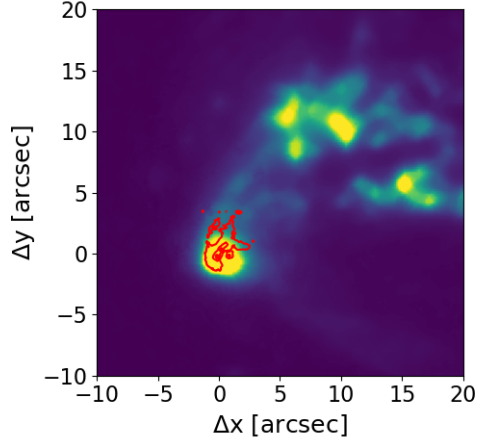


Figure 7. The background image shows the $[\text{O III}]\lambda 5007$ flux map from the MUSE-WFM data, which shows an overall asymmetric conical morphology with two distinct filaments on hundreds of parsec scales. The red contours show the $[\text{O III}]$ outflow morphology obtained from the NFM observations in the middle panel of Fig. 2. Comparing the NFM contours with that of the WFM $[\text{O III}]$ flux map, it appears that the two filaments observed in the WFM data have their origins in parsec-scale outflow traced with the NFM.

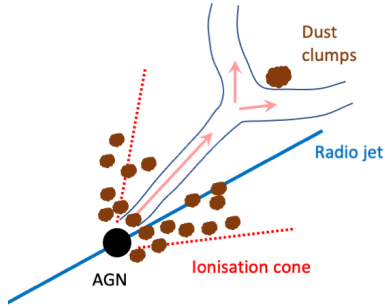


Figure 8. A cartoon model of the ionised outflow observed with the MUSE-NFM data in the Circinus galaxy. The outflow might be launched as a collimated structure by the radio jet, which then fragments into two filaments probably due to the presence of a dense clump at the tip of the collimated structure. The dust is distributed along the ionisation cone, apparent from the extinction maps and also consistent with archival mid-infrared observations.

axis of the ionisation cone. The relative orientations of the radio jet and the ionisation cone in the Circinus galaxy are depicted in Fig. 8.

The outflow itself is not composed of uniformly distributed ionised gas, but shows the presence of clumps, confirming previous observations from lower resolution data of other targets that the outflowing media are non-uniform in nature (e.g., Kakkad et al. 2018, 2022). The presence of clumps or knots along outflow/ionised gas filaments in the Circinus galaxy has also been previously reported in Veilleux & Bland-Hawthorn (1997) and these structures have been attributed to bow-shocked features that resemble Herbig Haro objects that interact strongly with the surrounding ISM. The observed morphology in the NFM data could be a smaller-scale version of the observations in larger scales.

The collimated component of the outflow most likely fragments into two components because of the presence of an obstruction in the path of the outflow. In the NFM data, there is an indication of the presence of a dust clump via extinction maps obtained from the

outflowing component of $\text{H}\alpha$ and $\text{H}\beta$ emission. Infrared observations targeting primarily the dust emission could confirm this scenario. Filament structures are also observed in images that trace gas across larger scales (e.g., Marconi et al. 1994; Veilleux & Bland-Hawthorn 1997) and it is probable that the NFM data presented in this paper reveals the origin of the kiloparsec-scale filaments. Fig. 7 shows the ionised gas morphology traced by the archival MUSE-WFM observations (background) and the emission from the outflowing $[\text{O III}]$ component from the MUSE-NFM data (red contours). The spatial distribution of the filaments observed in WFM is strongly suggestive that their origin is to be found in the fragmented arms of the tuning fork observed in the NFM observations.

Fig. 8 shows an overall cartoon model of the ionised outflow in the Circinus galaxy, that shows the ionised outflow that fragments into two filaments, probably due to the presence of a dense clump at the tip of the collimated structure. The dust itself is distributed around the ionisation cone and it envelops the lower velocity ionised gas within the conical structure. We speculate that the outflow itself might be launched due to the radio jet, which cannot be robustly confirmed based on the available archival radio observations, as mentioned earlier.

As the NFM observations have only recently targeted the nearby galaxies, it is unclear if such outflow structures and fragmentations within outflows are common. If this is indeed observed for majority of the galaxies, conventional outflow models that use ionisation cone morphology may need to be revised to account for the results from these high spatial resolution data.

6 SUMMARY & CONCLUSIONS

We presented the MUSE NFM observations of the Circinus galaxy at a spatial resolution of $0.1''$ (~ 2 pc) that resolves the regions close to the AGN torus. We derived the properties of the ionised gas outflow using the $[\text{O III}]\lambda 5007$ emission line and the dust distribution using Balmer Decrement. We follow a non-parametric approach to analyse the emission lines, so the derived properties are independent of the fitting functions used. The main results of this work is summarized below:

- The flux distribution of the systemic component of $[\text{O III}]$ emission, defined by the velocity components within $\pm 300 \text{ km s}^{-1}$, shows a conical morphology, which is also observed in larger spatial scales up to hundreds of parsecs in the literature. Archival radio observations show that the radio jet is aligned approximately with the edge of the ionisation cone. The flux distribution of the outflowing component of the $[\text{O III}]$ emission, on the other hand, shows a collimated structure up to ~ 30 pc before fragmenting into two arms that overall mimics a “tuning-fork” shape. The outflowing structure itself is not smooth and shows clumps at several locations.

- A comparison between the stellar kinematic map and the $[\text{O III}]$ centroid map suggests that the ionised gas (both the systemic as well as the outflowing component) co-rotates with the host galaxy. Both the non-parametric velocity distributions, v_{10} and w_{80} show similar structures as the outflow flux i.e., the tuning-fork shapes. Most of this outflow is blue-shifted, consistent with the outflow models of the Circinus galaxy reported in the literature.

- We find a total instantaneous mass outflow rate of $\sim 0.01 M_{\odot} \text{ yr}^{-1}$ (3×10^{-7} on average per pixel of size 0.5 pc) and a time-average mass outflow rate of $10^{-4} M_{\odot} \text{ yr}^{-1}$. This is much lower than the star formation within the galaxy and therefore, the ionised gas outflow is not expected to regular star formation within a radius of ~ 100 pc from the AGN location.

- The extinction maps using the systemic components of the H β and H α line show that the dust distribution is concentrated along the ionisation cone i.e., the polar direction, consistent with the archival mid-infrared observations. The extinction map obtained from the outflowing components of H β and H α shows a scarce distribution, with a clump approximately at the tip of the collimated part of the outflow. This dust clump might explain the fragmentation in the outflowing ionised gas.

- We combine previous reported results gathered from the literature and the observed outflows from the NFM data presented in this paper to present a model of the ionised gas outflow in the Circinus galaxy. We suggest that the observed outflow in the Circinus galaxy is composed of high velocity collimated gas that is enveloped by lower velocity dusty ionised gas. The presence of a dust clump at the tip of the collimated part of the outflow might be responsible for the fragmentation in the outflowing gas. The collimated outflow might be launched by a radio jet. Although the jet, observed in low spatial resolution radio observations, does not show a 1:1 alignment with the outflowing cone PA, they are known to bend and change at larger scales.

While the MUSE-NFM only provides the kinematic information in the ionised gas phase, outflows have been known to exist also in the molecular gas phase in the Circinus galaxy. A multi-wavelength approach to trace gas in the other phases such as warm and cold molecular, at the same spatial resolution of ~ 2 pc, will be key to obtaining a holistic view into the outflow-AGN connection in the Circinus galaxy. Furthermore, high spatial resolution radio observations will verify if the observed collimated outflow is a result of jet-ISM interaction on small scales.

ACKNOWLEDGEMENTS

We would like to thank the anonymous referee for insightful comments and suggestions to improve this manuscript. The authors also thank T. Fischer for useful discussions. Based on observations from the ESO programme ID 0103.B-0396. M.S. and S.K. acknowledge support by the Science Fund of the Republic of Serbia, PROMIS 6060916, BOWIE and by the Ministry of Education, Science and Technological Development of the Republic of Serbia through contract No. 451-03-9/2022-14/200002. D.A. acknowledges funding through the European Union's Horizon 2020 and Innovation programme under the Marie Skłodowska-Curie grant agreement no. 793499 (DUSTDEVILS).

DATA AVAILABILITY

The data presented in this paper is available with ESO archive under the programme ID: 0103.B-0396.

REFERENCES

Antonucci R., 1993, *ARA&A*, 31, 473
 Arévalo P., et al., 2014, *ApJ*, 791, 81
 Asmus D., 2019, *MNRAS*, 489, 2177
 Asmus D., Hönig S. F., Gandhi P., 2016, *ApJ*, 822, 109
 Bacon R., et al., 2010, in *Ground-based and Airborne Instrumentation for Astronomy III*. p. 773508, doi:10.1117/12.856027
 Baldwin J. A., Phillips M. M., Terlevich R., 1981, *PASP*, 93, 5
 Bock J. J., et al., 2000, *AJ*, 120, 2904

Braatz J. A., Wilson A. S., Gezari D. Y., Varosi F., Beichman C. A., 1993, *ApJ*, 409, L5
 Calzetti D., Armus L., Bohlin R. C., Kinney A. L., Koornneef J., Storchi-Bergmann T., 2000, *ApJ*, 533, 682
 Cappellari M., 2017, *MNRAS*, 466, 798
 Cappellari M., Emsellem E., 2004, *PASP*, 116, 138
 Combes F., et al., 2019, *A&A*, 623, A79
 Dimitrijević M. S., Popović L. Č., Kovačević J., Dačić M., Ilić D., 2007, *MNRAS*, 374, 1181
 Dullemond C. P., van Bemmell I. M., 2005, *A&A*, 436, 47
 Elitzur M., 2012, *ApJ*, 747, L33
 Elmouttie M., Haynes R. F., Jones K. L., Sadler E. M., Ehle M., 1998, *MNRAS*, 297, 1202
 Fischer T. C., Crenshaw D. M., Kraemer S. B., Schmitt H. R., 2013, *ApJS*, 209, 1
 Fonseca-Faria M. A., Rodríguez-Ardila A., Contini M., Reynaldi V., 2021, *MNRAS*, 506, 3831
 For B. Q., Koribalski B. S., Jarrett T. H., 2012, *MNRAS*, 425, 1934
 Freeman K. C., Karlsson B., Lynga G., Burrell J. F., van Woerden H., Goss W. M., Mebold U., 1977, *A&A*, 55, 445
 Gallimore J. F., Baum S. A., O'Dea C. P., 2004, *ApJ*, 613, 794
 Gallimore J. F., et al., 2016, *ApJ*, 829, L7
 García-Burillo S., et al., 2019, *A&A*, 632, A61
 García-Burillo S., et al., 2021, *A&A*, 652, A98
 García-González J., et al., 2017, *MNRAS*, 470, 2578
 Genzel R., et al., 2011, *ApJ*, 733, 101
 González Delgado R. M., Cerviño M., Martins L. P., Leitherer C., Hauschildt P. H., 2005, *MNRAS*, 357, 945
 Harrison C. M., Alexander D. M., Mullaney J. R., Swinbank A. M., 2014, *MNRAS*, 441, 3306
 Ho I. T., et al., 2016, *Ap&SS*, 361, 280
 Hönig S. F., 2019, *ApJ*, 884, 171
 Hönig S. F., Kishimoto M., 2017, *ApJ*, 838, L20
 Hönig S. F., Kishimoto M., Antonucci R., Marconi A., Prieto M. A., Tristram K., Weigelt G., 2012, *ApJ*, 755, 149
 Hönig S. F., et al., 2013, *ApJ*, 771, 87
 Isbell J. W., et al., 2022, *A&A*, 663, A35
 Jaffe W., et al., 2004, *Nature*, 429, 47
 Jarrett T. H., Cluver M. E., Brown M. J. I., Dale D. A., Tsai C. W., Masci F., 2019, *ApJS*, 245, 25
 Kaasinen M., Bian F., Groves B., Kewley L. J., Gupta A., 2017, *MNRAS*, 465, 3220
 Kakkad D., et al., 2016, *A&A*, 592, A148
 Kakkad D., et al., 2018, *A&A*, 618, A6
 Kakkad D., et al., 2020, *A&A*, 642, A147
 Kakkad D., et al., 2022, *MNRAS*, 511, 2105
 Kauffmann G., et al., 2003, *MNRAS*, 346, 1055
 Kewley L. J., Dopita M. A., Sutherland R. S., Heisler C. A., Trevena J., 2001, *ApJ*, 556, 121
 Kreckel K., et al., 2018, *ApJ*, 863, L21
 Leftley J. H., Tristram K. R. W., Hönig S. F., Kishimoto M., Asmus D., Gandhi P., 2018, *ApJ*, 862, 17
 López-Gonzaga N., Burtscher L., Tristram K. R. W., Meisenheimer K., Schartmann M., 2016, *A&A*, 591, A47
 Lopez-Rodriguez E., et al., 2020, *ApJ*, 893, 33
 Marconi A., Moorwood A. F. M., Origlia L., Oliva E., 1994, *The Messenger*, 78, 20
 Marin F., Goosmann R. W., Gaskell C. M., 2015, *A&A*, 577, A66
 Matt G., Fabian A. C., Guainazzi M., Iwasawa K., Bassani L., Malaguti G., 2000, *MNRAS*, 318, 173
 Mingozzi M., et al., 2019, *A&A*, 622, A146
 Nenkova M., Ivezić Ž., Elitzur M., 2002, *ApJ*, 570, L9
 Netzer H., 2015, *ARA&A*, 53, 365
 Osterbrock D. E., Ferland G. J., 2006, *Astrophysics of gaseous nebulae and active galactic nuclei*
 Ramos Almeida C., Ricci C., 2017, *Nature Astronomy*, 1, 679
 Rupke D. S., Veilleux S., Sanders D. B., 2005, *ApJS*, 160, 87
 Sanders R. L., et al., 2016, *ApJ*, 816, 23

- Stalevski M., Ricci C., Ueda Y., Lira P., Fritz J., Baes M., 2016, *MNRAS*, **458**, 2288
- Stalevski M., Asmus D., Tristram K. R. W., 2017, *MNRAS*, **472**, 3854
- Stalevski M., Tristram K. R. W., Asmus D., 2019, *MNRAS*, **484**, 3334
- Toba Y., et al., 2021, *ApJ*, **912**, 91
- Tristram K. R. W., et al., 2007, *A&A*, **474**, 837
- Tristram K. R. W., Burtscher L., Jaffe W., Meisenheimer K., Hönig S. F., Kishimoto M., Schartmann M., Weigelt G., 2014, *A&A*, **563**, A82
- Urry C. M., Padovani P., 1995, *PASP*, **107**, 803
- Veilleux S., Bland-Hawthorn J., 1997, *ApJ*, **479**, L105
- Veilleux S., Osterbrock D. E., 1987, *ApJS*, **63**, 295
- Veilleux S., Maiolino R., Bolatto A. D., Aalto S., 2020, *A&ARv*, **28**, 2
- Venanzi M., Hönig S., Williamson D., 2020, *ApJ*, **900**, 174
- Virtanen P., et al., 2020, *Nature Methods*, **17**, 261
- Weilbacher P. M., Streicher O., Urrutia T., Pécontal-Rousset A., Jarno A., Bacon R., 2014, in Manset N., Forshay P., eds, *Astronomical Society of the Pacific Conference Series Vol. 485, Astronomical Data Analysis Software and Systems XXIII*. p. 451 ([arXiv:1507.00034](https://arxiv.org/abs/1507.00034))
- Weilbacher P. M., et al., 2020, *A&A*, **641**, A28
- Wylezalek D., Flores A. M., Zakamska N. L., Greene J. E., Riffel R. A., 2020, *MNRAS*, **492**, 4680
- Zschaechner L. K., et al., 2016, *ApJ*, **832**, 142

This paper has been typeset from a $\text{\TeX}/\text{\LaTeX}$ file prepared by the author.